Cardiac AAV9:PKP2 Gene Therapy Reduces Ventricular Arrhythmias, Reverses Adverse Remodeling, and Reduces Mortality in a Mouse Model of ARVC

Iris Wu
Tenaya Therapeutics
Amara Greer-Short
Tenaya Therapeutics
Alex Aycinena
Tenaya Therapeutics
Anley Tefera
Tenaya Therapeutics
Reva Shenwai
Tenaya Therapeutics
Farshad Farshidfar
Tenaya Therapeutics
Melissa Van Pell
Tenaya Therapeutics
Emma Xu
Tenaya Therapeutics
Chris Reid
Tenaya Therapeutics
Neshel Getuiza
Tenaya Therapeutics
Beatriz Lim
Tenaya Therapeutics
Tae Won Chung
Tenaya Therapeutics
Renee Butler
Tenaya Therapeutics
Stephanie Steltzer
Tenaya Therapeutics
Jaclyn Ho
Tenaya Therapeutics https://orcid.org/0000-0001-9166-5953

Kristina Green
Tenaya Therapeutics
Kathryn Ivey
Tenaya Therapeutics
Timothy Hoey
Tenaya Therapeutics
Jin Yang
Tenaya Therapeutics
Aliya Zeng
Tenaya Therapeutics
Zhihong Yang
jane.yang@tenayathera.com

Tenaya Therapeutics

Article

Keywords:

Posted Date: May 24th, 2023

DOI: https://doi.org/10.21203/rs.3.rs-2958419/v1

Additional Declarations: There is **NO** Competing Interest.

Version of Record: A version of this preprint was published at Communications Medicine on March 18th, 2024. See the published version at https://doi.org/10.1038/s43856-024-00450-w.

Cardiac AAV9:PKP2 Gene Therapy Reduces Ventricular Arrhythmias, Reverses Adverse Right Ventricular Remodeling, Improves Heart Function, and Reduces Mortality in a *Pkp2*-deficient Mouse Model of Arrhythmogenic Right Ventricular Cardiomyopathy

Iris Wu[1*], Aliya Zeng[1*], Amara Greer-Short[1], J. Alex Aycinena[1], Anley E. Tefera[1], Reva Shenwai[1], Farshad Farshidfar[1], Melissa Van Pell[1], Emma Xu[1], Chris Reid[1], Neshel Getuiza[1], Beatriz Lim[1], Tae Won Chung[1], Renee Butler[1], Stephanie Steltzer[1], Jaclyn Ho[1], Kristina Green[1], Kathryn N. Ivey[1], Timothy Hoey[1], Jin Yang[1], Zhihong Jane Yang[1**]

[1]Tenaya Therapeutics, South San Francisco, CA 94080, USA

* These two authors contributed equally.

** Senior correspondent, E-mail: jane.yang@tenayathera.com

Abstract

Arrhythmogenic right ventricular cardiomyopathy (ARVC) is a familial cardiac disease associated with ventricular arrhythmias and an increased risk of sudden cardiac death. Currently, there are no approved treatments that address the underlying genetic cause of this disease. Mutations in desmosome gene *Plakophilin-2 (PKP2*) account for 45% of ARVC cases and result in reduced gene expression. Our goal is to examine the feasibility and the efficacy of adeno-associated virus 9 (AAV9)-mediated restoration of PKP2 expression in a cardiac specific knock-out mouse model of *Pkp2*. We demonstrated that a single-dose cardiac AAV9:PKP2 gene delivery effectively prevented disease development before overt cardiomyopathy and attenuated disease progression after overt cardiomyopathy. Restoration of *PKP2* expression leads to highly coordinated and durable correction of *PKP2*-associated transcriptional networks beyond desmosomes, revealing a broad spectrum of biological perturbances behind ARVC disease etiology. These results indicate that cardiac AAV9:PKP2 gene therapy may be a promising therapeutic approach to treat ARVC patients with *PKP2* mutations.

Main

Arrhythmogenic right ventricular cardiomyopathy (ARVC) or arrhythmogenic cardiomyopathy (ACM) is an inherited heart disease characterized by ventricular arrhythmias and progressive cardiac dysfunction (Corrado et al., 2020; Gandjbakhch et al., 2018; Gemayel et al., 2001; Sen-Chowdhry et al., 2004; Zipes, et al., 2006). Clinical presentation of ARVC varies from a concealed early phase, a later manifestation of lethal ventricular arrhythmias, and ultimately heart failure that requires heart transplant (Basso et al., 2009; Corrado et al., 2017; Gemayel et al., 2001). ARVC has an estimated prevalence in the general population of 1:1000 to 1:5000 with the mean age of presentation before 40 years old (Basso et al., 2011; Groeneweg et al., 2015; Dalal et al., 2005; Nava et al., 2000; Hulot et al., 2004). Arrhythmic sudden cardiac death (SCD) could be the first symptom, often diagnosed postmortem, of mostly young and athletic patients (Corrado et al., 2017; Finocchiaro et al., 2016;).

Mutations in the desmosome gene *Plakophillin-2*, *PKP2*, are the most frequent cause of genetic ARVC and account for approximately 43% of ARVC cases (Choudhary et al., 2016, Dries et al., 2021; Jacob et al., 2012; van Tintelen et al., 2006; Walsh et al., 2017). Desmosomes are adhesive intercellular connections that play critical roles in heart development and performance (Kowalczyk and Green, 2013; Vermij et al., 2017). Interactions among desmosome proteins ensure proper structural anchoring and organization of intermediate filaments, cardiac sarcomere, and other organelles (Delmar and McKenna, 2010; Sheikh et al., 2009). Mutations in the *PKP2* gene are heterozygous in patients and lead to haploinsufficiency in PKP2 protein levels (Akdis et al., 2016; Asimaki et al., 2009; Chen et al., 2014; Kohela et al., 2021; Rasmussen et al., 2014). Reduction of PKP2 protein at the intercalated discs (ID) disrupts desmosomes and other ID structures such as gap junctions (GJs) (Basso et al., 2011; Delmar and McKenna, 2010; Vermij et al., 2017). Reduction of Connexin 43 (Cx43), a critical component of GJs, results in compromised electrical coupling and heterogeneous conduction between cardiomyocytes (Oxford et al., 2007; Rodriguez-Sinovas et al., 2021). These structural corruptions trigger cell death response, inflammatory infiltration, and metabolic perturbation that underpin clinical manifestations of electrical instability, cardiac structural deterioration, fibrofatty infiltration, and heart failure (Asatryan et al.

2021; Austin et al., 2019; Cerrone et al., 2017; Chen et al., 2014; Dubash et al., 2016; Pérez-Hernández et al., 2022; Reichart et al., 2022; Song et al., 2020; Zhang et al., 2021).

Clinical management of ARVC patients includes lifestyle modification, pharmacological treatment, catheter ablation, ICDs, and heart transplantation (Calkins et al., 2017; McKenna, 2022). So far, there is no approved treatment that addresses the underlying genetic cause of this disease. It is technically challenging to apply conventional therapeutic approaches to restore defective large cellular structures such as the desmosome and manage their pleiotropic impact on complex signaling networks. Therefore, a new treatment paradigm that targets the underlying genetic cause of the disease is needed to manage the multiplicity of disease manifestations during disease onset and progression.

In this study, both *PKP2*-deficient human induced pluripotent stem cell-derived cardiomyocytes (iPSC-CMs) and a cardiac-specific knock-out, *Pkp2-cKO*, mouse model were utilized to identify the molecular, structural, and functional signatures that recapitulate human ARVC clinical phenotypes. Using the *in vivo* mouse model, we examined the feasibility and the efficacy of gene replacement by AAV9-mediated exogenous restoration of PKP2. This is the first study demonstrating that ARVC clinical phenotypes, recapitulated by a mouse model, 1) were largely preventable before overt cardiomyopathy and 2) can be attenuated to stop or slow down progression to heart failure by exogenous restoration of PKP2 expression. Restoration of PKP2 expression led to a highly coordinated and durable correction of structural genes encoding desmosome, sarcomere, and Ca^{2+}-handling system, and corrections of multiple signaling pathways of metabolism, inflammation, and apoptosis. Our studies reveal that the desmosome is a fundamental molecular building block in maintaining cellular integrity and functions of cardiomyocytes and heart. We propose that cardiac AAV9:PKP2 could be a beneficial gene therapy approach to reduce ventricular arrhythmias, reverse adverse right ventricular remodeling, improve heart function, and reduce mortality in ARVC patients with *PKP2* mutations. TN-401, Tenaya's AAV9:PKP2

clinical drug candidate, is currently advancing in Investigational New Drug (IND)-enabling studies.

Results

AAV:PKP2 corrected disease phenotypes in a human iPSC-CM model

To model ARVC disease and identify the molecular, structural, and functional signatures that are fundamental to the disease mechanisms, we carried out RNA sequencing analyses of iPSC-CMs after acute silencing of *PKP2* expression. These studies revealed that the desmosome functions as a signaling hub connecting key structures (Agullo-Pascual et al., 2014) in cardiomyocytes such that reduction in *PKP2* expression led to down-regulation of structural and functional gene expression encoding components of desmosomes, sarcomeres, intermediate filaments, and ion channels (Figure 1a). Down-regulation of protein or mRNA was shown for desmoplakin (DSP), plakoglobin (JUP), myosin-binding protein C3 (MyBPC3), desmin (DES), and sodium voltage-gated channel α subunit 5 (*SCN5A*) (Figure 1b). PKP2 deficiency resulted in structural disappearance of PKP2 and DSP from the cellular membrane and caused cell-to-cell disarray of patterned iPSC-CMs (Figure 1c). In addition, PKP2 deficiency perturbed both contractile (Figure 1d) and electrophysiological properties of iPSC-CMs (Figure 1e).

The 1st generation AAV expression cassette was used for iPSC-CM-based studies and the 2nd generation for *in vivo* mouse efficacy studies (Figure 2a). Dose-dependent protein expression was evident in iPSC-CMs driven by a cardiac-specific troponin T promoter (Figure 2b). AAV:human PKP2 (AAV:hPKP2), which is a AAV9 variant engineered to have a higher transduction efficiency to iPSC-CMs than AAV9, restored DSP expression post *PKP2* silencing when compared to the reduced DSP protein without AAV rescue (Figure 2c). AAV:hPKP2 restored contractility as quantified by contraction velocity when compared to the reduced contraction velocity without AAV rescue (Figure 2d). Using human iPSC-CMs as a cell model for ARVC, AAV:hPKP2

restored desmosomes and rescued contractility in PKP2-deficient iPSC-CMs, suggesting PKP2 governs intrinsic cellular properties of cardiomyocytes.

Pkp2-cKO ARVC mouse model recapitulated the majority of human ARVC clinical manifestations

We used a mouse conditional knockout model to assess the feasibility and the efficacy of AAV-mediated *PKP2* gene replacement. Consistent with the early observations of this model (Cerrone et al., 2017), tamoxifen-induced cardiac deletion of both alleles of *Pkp2* in adult mice at 1 week did not show overt structural and functional changes. Weekly monitoring and tissue collection at the end of the study showed disruption of desmosomes and GJs (Figure 3a), severe spontaneous premature ventricular contractions (PVCs) (Figure 3b), biventricular dilatation (Figure 3c), and a sharp decline in cardiac function (Figure 3d) and survival (Figure 3e) after 3-4 weeks of induced cardiac knock-out of *Pkp2*. These phenotypes recapitulated human ARVC clinical manifestations. However, unlike in humans, heterozygous disruption of *Pkp2* in mouse hearts did not result in cardiac phenotypes that closely recapitulated human ARVC symptoms (Cerrone et al., 2012; van Opbergen et al., 2019). Thus, homozygous *Pkp2-cKO* mouse was used as a model of human ARVC.

AAV9:PKP2 treatment largely attenuated disease development and disease progression to mortality in *Pkp2-cKO* ARVC mouse

To determine whether the AAV9 expression cassette (Figure 2a, the 2nd generation) encoding either the human *PKP2* or the mouse ortholog could counteract the effects of cardiac *Pkp2* gene deletion, *Pkp2-cKO* mice were given a single systemic dose of TN-401 (AAV9: human PKP2) or AAV9:mPkp2 (AAV9:mouse Pkp2) 3 weeks prior to tamoxifen induction of cardiac *Pkp2* gene deletion (Figure 4a). Hank's Balanced Salt Solution (HBSS) was administered as vehicle control to WT control animals and to AAV-untreated *Pkp2-cKO* animals. At 4 weeks post gene deletion and 7 weeks post AAV delivery, both human and mouse orthologs prevented ventricular arrhythmia event

frequency and severity as summarized by a ventricular arrhythmia score (Figure 4b, Suppl. Table 1), right ventricular remodeling (Figure 4c), and decline in left ventricular function (Figure 4d), which were prominent features of *Pkp2-cKO* mice at this timepoint. TN-401 demonstrated significant efficacy in preventing ARVC development and in extending median lifespan by ≥ 58 weeks, far beyond the 4.7 weeks observed in the HBSS-treated *Pkp2-cKO* animals, with survival comparable to the natural lifespan of the WT control animals as monitored up to 72 weeks (Figure 4e). In this same study, we also evaluated efficacy of AAV9:mPkp2 in *Pkp2-cKO* mice at 3 intervention timepoints and concluded that there were no significant differences in efficacy readouts of EF, RV dilation, arrhythmias, and prolonged lifespan of more than 50% of the treated animals by 50 weeks (Suppl. Figure 1). Overall, these results showed that either the human PKP2 or the mouse ortholog was sufficient to prevent the detrimental cardiac and survival phenotypes of *Pkp2-cKO* mice when delivered in the AAV9 vector.

To assess the dose response to TN-401, *Pkp2-cKO* mice were given single systemic treatments one week after tamoxifen induction of cardiac *Pkp2* gene deletion (Figure 5a) and sacrificed at 4 weeks post induction (3 weeks post AAV treatment) for histological and expression analyses. TN-401 treatment of *Pkp2-cKO* mice showed dose-dependent efficacy in reducing RV dilation as estimated by RV area normalized to body weight, in preventing decline of LV ejection fraction, and a trending dose-dependent reduction in arrhythmias (Figure 5b). At molecular level, left ventricle heart tissue showed dose-dependent protein expression of human PKP2 (Figure 5c, top panel) as well as dose-dependent restoration of DSP and JUP, two additional desmosome proteins that were decreased in *Pkp2-cKO* mice (Figure 5c, bottom two panels). Connexin 43 (Cx43), a gap junction protein present at intercalated discs, was reduced in *Pkp2-cKO* mice, as shown by immunohistochemistry of heart tissue, and was restored in *Pkp2-cKO* mice treated with TN-401 (Figure 5d, top row). TN-401 treatment also significantly reduced fibrosis development and collagen deposition in both right ventricle and left ventricle (Figure 5d, bottom row and quantification shown in the graph). In addition, quantitative analyses of molecular signatures supported that

TN-401 treatment reduced mRNA expression of heart failure markers, fibrosis, and tissue remodeling genes in both left and right ventricles (Figure 5e, LV data not shown).

Overall, TN-401 treatment supported a dose-dependent improvement in ARVC phenotypes and efficacy in the *Pkp2-cKO* mouse model of ARVC. TN-401 in this dose-escalation study demonstrated efficacy at doses ≥ 3E13 vg/kg in preventing adverse right ventricular remodeling, and improving ventricular function, fibrosis, and electrophysiological properties.

The preventive mode of treatment, dosing before overt structural changes, demonstrated significant benefit of early intervention in largely preventing disease development and extending lifespan. To further examine whether ARVC disease progression could be slowed down or attenuated by restoration of PKP2 expression after overt structural changes, the therapeutic mode of treatment, we dosed animals at 2.5 weeks after inducing cardiac knock-out of *Pkp2* (Figure 6a), when overt structural changes, such as RV dilatation had occurred. AAV9:mPkp2 treatment reversed right ventricle enlargement (Figure 6c), prevented further decline of the left ventricle function (Figure 6d), and attenuated the progression of arrhythmias (Figure 6e). Significantly, PKP2 gene therapy blunted early development of heart failure and reduced mortality of this mouse model of ARVC throughout one year follow-up with a median lifespan by ≥ 50 weeks (Figure 6b).

Restoration of *PKP2* expression led to a highly coordinated and durable correction of *PKP2*-associated transcriptional networks beyond desmosomes

It was rather surprising to observe that restoration of a single desmosome component, PKP2, led to significant survival benefits, improved cardiac function, reversed adverse RV remodeling, reduced ventricular arrhythmias, and prevented fibrosis. We asked whether “on-target” PKP2 effects possibly extend beyond its effects on the desmosome by evaluating PKP2 dose-dependent response, specifically at the transcriptional level.

To our knowledge, there is no reported study that reveals whether 1) PKP2 dynamically coordinates its gene expression with other desmosome members, and 2) to what extent PKP2 quantitively dictates the state of disease progression. To obtain a deeper understanding, two large-scale RNA sequencing analyses were conducted.

Pkp2-cKO mice were given a single systemic dose of TN-401 one week before tamoxifen induction of cardiac *Pkp2* gene deletion (Figure 7a) and cardiac function and arrhythmias were evaluated at 4 and 9 weeks post induction. Mice were sacrificed at 9 weeks post induction and heart tissues were collected for RNA sequencing and quantification of PKP2 RNA and protein expression. At a 2-fold expression difference between low, 3E13 vg/kg and high, 6E13 vg/kg doses at 9 weeks (Figure 7b), we did not observe any significant dose-dependent difference in key readouts of EF%, RV dilatation, and arrhythmia score, although the less critical readouts of LV mass to body weight and QT intervals did show dose dependence and one out of six animals at the high dose vs 5 out of nine animals at the low dose had arrhythmia scores ≥1 at 9 weeks post induction (Figure 7c). We decided to evaluate specific gene classes including desmosome, gap junctions (GJs), sarcomere, ion channels and Ca^{2+} handling systems, heart failure markers, and fibrosis, that have been previously demonstrated to be significant contributors to disease mechanisms (Figure 7d) (Asatryan et al. 2021; Austin et al., 2019; Cerrone et al., 2017; Chen et al., 2014; Dubash et al., 2016; Pérez-Hernández et al., 2022; Reichart et al., 2022; Song et al., 2020; Zhang et al., 2021). Comparison between WT vs HBSS treated *Pkp2-cKO* animals showed significant changes in gene expression in these classes and an extensive reversal of these changes in response to TN-401 (Figure 7e, genes of interest marked in red). Intriguingly, RNA sequencing analysis at the transcriptional level showed a positive dose correlation to TN-401 among structural genes encoding desmosomes, Cx43, sarcomeres, ion channels and Ca^{2+} handling proteins (Figure 7f). When examining expression of heart failure markers and fibrosis genes, we noticed a negative dose correlation to TN-401 (Figure 7f). Therefore, while key functional readouts of efficacy could not be distinguished between dose levels of 3E13 and 6E13 vg/kg, the 2-fold difference in PKP2 transcript levels achieved by these two doses did result in

quantitative and dose-dependent changes in transcriptional signatures described above. Based on this observation, we believe that identification of key genes can be informative in associating a transcriptional signature with a particular phase of ARVC disease progression and therefore, may facilitate patient stratification in a more quantitative and precise manner, particularly in early 'concealed' phase when structural changes are not evident.

Previous transcriptome analysis showed that TN-401 restored expression of structural genes and attenuated expression of genes encoding adverse remodeling factors in a highly coordinated and quantitative fashion. We asked whether such transcriptional response can be sustained to attenuate disease progression and therefore, extend survival over a longer duration.

As shown earlier in Figure 6, a single dose of AAV9:mPkp2 treatment after overt cardiomyopathy halted disease progression via reversed adverse right ventricular remodeling, improved LV function, prevented arrhythmia from worthening, and extended median lifespan by ≥ 50 weeks post induction of *Pkp2* deletion. Heart tissues collected at 51 weeks post induction of *Pkp2* deletion were analyzed by RNA sequencing (Figure 8a). Compared to intervention before overt structural changes (the preventive mode), AAV9:mPkp2 intervention after overt structural change (the therapeutic mode) showed comparable efficacy in extending life span at the same dose, 1E14 vg/kg (Figure 8b). Principle Component Analysis (PCA) (Jollife and Cadima, 2016) showed that transcriptional profiles of AAV9:mPkp2-treated *Pkp2-cKO* animals were clustered close to WT and distant from non-treated animals, suggesting a normalization of transcriptional landscape close to WT in response to the treatment (Figure 8c). While the transcriptional profile of low-dose treated animals showed a partial recovery pattern, the transcriptional profiles of the high-dose treated animals effectively overlapped with that of WT samples (Figure 8c). In addition, when comparing the total number of differentially up- or down-regulated genes relative to the WT animals, the preventive mode and to a lesser degree, the therapeutic mode of intervention showed a significant normalization compared to that between *Pkp2-cKO* and WT animals (Figure 8d). When

comparing HBSS-treated *Pkp2-cKO* animals vs WT, the significant negatively enriched gene sets identified by Gene Set Enrichment Analysis (GSEA) (Subramanian et al., 2005) were mitochondrial dysfunction, cardiac muscle contraction, and cardiac muscle conduction. The top significant positively enriched gene sets were predominantly fibrosis related. Both modes of intervention showed significant reversal of these enriched gene sets with the preventive mode supporting the most complete reversal (Figure 8e). To our surprise, the long-term survival benefit offered by either mode of intervention was supported by a broad spectrum of sustained correction of gene expression encoding components of the desmosomes, sarcomeres, ion channels and calcium handling systems, and also multiple pathways that regulate metabolism, fibrosis, inflammation, and apoptosis as shown (Figure 8f and 8g). Once again, both modes of intervention showed significant reversal of these enriched gene sets with the preventive mode effect being most complete (Figure 8g). Quantitative RT-PCR validated that at the same dose, 1E14 vg/kg, each mode of intervention maintained a similar level of *Pkp2* transgene expression at 51 weeks, suggesting the mode of intervention does not change the durability of the transgene expression (Figure 8h). Expression of heart failure genes (*Nppa* and *Nppb*) and fibrosis genes (*Timp1, Col1a1,* and *Col3a1*) were significantly lowered by both modes of treatments at 1E14 vg/kg. In agreement with the observation shown by RNA-seq analyses, these genes were expressed higher in therapeutic mode than in the preventive mode among age-matched animals.

We concluded that long-term restoration of PKP2 expression by gene replacement approach was correlated with sustained restoration of a broad spectrum of structural genes and pathways, supporting a notion that early intervention is the key to restore PKP2-associated intrinsic transcriptional networks and their functions and therefore, increase overall cardiomyocyte fitness to effectively mitigate adverse maladaptive remodeling such as fibrosis as early as possible. These results strongly support that PKP2-associated transcriptional networks can be used to quantitively evaluate the extent of disease progression and gene therapy efficacy at the molecular level.

More than 10x of efficacious dose of TN-401 proved to be safe in WT CD1 mice.

Safety evaluation of TN-401 in WT mice for 6 weeks (Figure 9a) showed no adverse effects at ≥ 10x efficacy dose on body weight (Figure 9b), heart weight and ventricular functions (Figure 9c), neutrophil to lymphocyte ratio (Figure 9d), liver weight and enzyme levels (Figure 9e), and platelet count and hemoglobin levels (Figure 9f). Histological analyses showed no TN-401-related changes in heart, lung, liver, pancreas, brain, kidneys, and skeletal muscle examined (data not shown).

Discussion

Our preclinical results demonstrated that AAV9-based PKP2 gene replacement approach can offer significant survival benefit in repairing cellular structures of desmosome, GJs, and Ca^{2+}-handling system, improving cardiac function, reducing ventricular arrhythmia event frequency and severity, and preventing adverse fibrotic remodeling in a dose-dependent fashion in a cardiac-specific *Pkp2* knock-out mouse model of ARVC.

About 50% of ARVC patients carry a genetic mutation in desmosome genes and half of this patient population carries mutations in *PKP2*. The heterogeneity of clinical symptoms of ARVC indicates genetic composition, maladaptive remodeling, environmental factors, lifestyle, and other unknown factors of individuals that likely affect disease onset and progression. Although mutations in desmosome genes have been confirmed as an underlying genetic cause of ARVC by large-scale prevalence studies (Choudhary et al., 2016, Dries et al., 2021; Jacob et al., 2012; Walsh et al., 2017), current understanding of the genetic background of this disease is limited and compounded by non-genetic factors and missing molecular links between defective desmosomes and disease development. Using both iPSC-CM and cardiac-specific *Pkp2-cKO* mouse models of ARVC and AAV9-mediated restoration of PKP2 expression, this is the first study to demonstrate that PKP2 is the essential genetic determinant underpinning 1) intrinsic cellular properties of cardiomyocytes; 2) disease onset based on the preventive mode of efficacy studies that proved AAV9:PKP2 effect to be dose-dependent with significant prevention of multiple disease phenotypes (Figures 4, 5, 7, and 8); 3) disease progression based on the therapeutic mode of efficacy study that showed reversal of right ventricle enlargement, halted decline of left ventricle function, attenuation of arrhythmia worsening, and most importantly, reduction of mortality (Figures 6 and 8).

Heterozygous PKP2 mutations in humans are predominantly truncation mutations resulting from nonsense, frameshift, or splice-site mutations (Awad et al., 2008; Gerull et al., 2004; Towbin et al., 2019). *PKP2* mRNAs containing premature stop codons are

subjected to surveillance and degradation by nonsense-mediated decay (NMD) machinery (Hug et al., 2016; Mura et al., 2013; Rasmussen et al., 2014). Degradation of the mutated mRNA results in haploinsufficiency as shown by reductions of both mRNA and protein in ARVC patients heart tissues from autopsy, endomyocardial biopsy or explants (Akdis et al., 2016; Asimaki et al., 2009; Kohela et al., 2021; Rasmussen et al., 2014). The preventive efficacy studies demonstrated that restoration of PKP2 expression correlated with restoration of function in a dose-dependent fashion, suggesting that the cellular level of PKP2 precisely and quantitatively dictates a relationship between the cellular input vs the functional outputs under the condition that is minimally influenced by other undefined genetic and nongenetic factors. This precise dose-function correlation of PKP2 possibly addresses the functional consequence of haploinsufficiency in real human cases and further supports the rationale of an AAV-based gene replacement approach. Furthermore, the RNA sequencing analyses revealed a broad spectrum of functional impact by PKP2 deficiency and destruction of desmosomes. These results strongly support a gene therapy-based intervention that addresses the root cause and its associated pleiotropism. Mutations in other desmosome genes also lead to destruction of the desmosome, suggesting mechanisms we observed here are likely applied similarly to other desmosome genes in their role of regulating dynamics of desmosome and other multi-united structures such as GJs, sarcomere, and the Ca^{2+}-handling system.

It is significant that restoration of a single component of the desmosome, PKP2, led to significant survival benefits of improved cardiac function, reversed adverse RV remodeling, reduced ventricular arrhythmias, and prevented fibrosis. This study demonstrated that “on-target” PKP2 effects extend beyond the desmosomes, at the transcriptional level, to other larger structures or pathways. Considering these data, we believe desmosomes dynamically tune and coordinate gene expression of all its components and quantitatively dictate the state and extent of ARVC disease progression as supported by dose dependency of PKP2. Our study showed that restoration of PKP2 leads to a highly coordinated and durable restoration of structural genes encoding desmosome, sarcomere, and Ca^{2+}-handling system components,

supporting the desmosome as a fundamental molecular regulatory hub in maintaining cellular integrity and function of cardiomyocytes and the heart, overall. These data further support that an early intervention by gene therapy before overt structural change could project a better prognostic outcome by restoring molecular structures to maintain overall fitness of cardiomyocytes and to prevent irreversible changes that could compromise the efficacy of gene therapy. These irreversible changes were investigated in our studies as both preventive and therapeutic modes of intervention showed significant reduction of enriched fibrosis gene sets. However, reduction of fibrosis by the therapeutic mode was to a lesser extent with concomitant expression of heart failure genes, *Nppa* and *Nppb* (Figure 8e). The sustained expression of *Nppa* and *Nppb* in the therapeutic mode of intervention might support observations that the natriuretic peptides encoded by *Nppa* and *Nppb* were functionally implicated in cardiac antifibrotic effects (Kerkela et al., 2015). Significantly, both modes of intervention showed comparable survival benefit, dramatically extending lifespan.

We did not have age-matched animals that were 51 weeks old and were induced for 2.5 weeks of gene deletion. It would be informative to understand the extent of secondary maladaptive remodeling that occurred after overt cardiomyopathy at 2.5 weeks post induction of gene deletion as the baseline for our therapeutic mode of intervention. This would allow us to determine whether the secondary maladaptive effects responded to the long-term treatment or to evaluate disease regression with pre-existing overt structural changes.

Cardiomyocyte loss due to atrophy or apoptosis puts unique challenges on what might or might not be responsive to therapeutic interventions in adult heart tissue. However, it is intriguing to see proposed reversibility of secondary maladaptive remodeling due to an overall long-term improvement of cardiac performance (Edelberg et al., 2022). The long-term effects by gene replacement targeting cardiomyopathy remain unknown in terms of its potential for disease reversibility. Surprisingly, in our studies, long-term AAV9:PKP2 treatment after overt RV dilatation showed an increased expression of genes underlying sarcomere organization (Figure 8g, middle panel). This transcriptional

signature could suggest a mechanism of partial regression of adverse structural remodeling due to enhanced sarcomere function in surviving cardiomyocytes. We are currently investigating this possibility.

Using a cardiac KO mouse model of ARVC, we identified fundamental mechanisms behind disruption of PKP2-assocated desmosome function and revealed its broad impact at the transcriptional level on GJs, sarcomere, ion channels and Ca^{2+} handling systems, and multiple pathways that critically regulate metabolism, inflammation, apoptosis, and fibrosis. These studies highlight the importance of identifying key transcripts in characterizing ARVC disease state and disease progression in a more quantitative and precise manner. Our efficacy data with PKP2 gene therapy and mechanistic analyses shed more light on understanding ARVC etiology and in practice, may help patients and physicians to make decisions regarding disease management and treatment.

Methods

Animal studies

Animal studies were performed according to Tenaya Therapeutics' animal use guidelines. The animal protocols were approved by the Institutional Animal Care and Use Committee and accredited by the Association for Assessment and Accreditation of Laboratory Animal Care (IACUC number: 2020.007).

Mouse model

Tenaya licensed a novel cardiomyocyte-specific, tamoxifen-activated *Pkp2-cKO (αMHC-Cre-ER(T2)/Pkp2$^{fl/fl}$)* mouse line in the C57BL/6 background from Dr. Mario Delmar, NYU Grossman School of Medicine (Ref). The *Pkp2-cKO* animals were induced with tamoxifen at 0.1mg/g for 3 consecutive days. TN-401 or AAv9:mPkp2 was given as a single dose via retro-orbital injection before or after animals were induced with tamoxifen. HBSS, as vehicle control, was injected to WT or non-AAV treated *Pkp2-cKO* animals. Tamoxifen injection activates Cre recombinase in Cre-positive animals and induces homozygous deletion of *Pkp2* gene. *Pkp2$^{fl/fl}$ Cre*-negative littermates were used as controls.

AAV virus production

AAV production was carried out as previously described (Reid et al., 2017). Briefly, HEK293T cells were seeded in a Corning HyperFlask (New York, NY) and triple transfected using a 2:1 PEI:DNA ratio (PEI Max) with a helper plasmid containing adenoviral elements (pHelper), a plasmid containing the Rep2 and Cap genes from the respective AAV serotype, and finally an ITR containing plasmid to be packaged. Three days following transfection cells were harvested and lysed. Virus was purified using iodixanol ultracentrifugation and cleaned and concentrated in Hank's Balanced Salt Solution (HBSS) + 0.014% Tween-20 using a 100-kDa centrifuge column (Amicon, Darmstadt, Germany). AAV was titered using either a PicoGreen or ddPCR assay.

iPSC-CM culture

iCell Cardiomyocytes2 were thawed according to the manufacturer's instructions (FUJIFILM Cellular Dynamics) and seeded onto Matrigel-coated plates at a density of 20,000 cells per well of 96-well plates or at a seeding density proportional to the well size. A total of 5 million iPSC-CM flooded 3X patterned 4Dcell 35 mm dish. Seeded cells were maintained in CDI maintenance media (FUJIFILM Cellular Dynamics) for 7-10 days until the days of treatments.

siRNA knockdown and AAV transduction

To knock down endogenous *PKP2* expression, four independent siRNAs were tested to confirm silencing at both mRNA and protein level at time points of 2, 4, 6, and 8 days (Silencer Select Pre-Designed siRNA, Invitrogen). A pool of two independent siRNAs were selected to transfect iPSC-CMs at a final concentration of 1.25 or 5 nM using Lipofectamine RNAiMAX (Thermo Fisher Scientific) in CDI maintenance media. Forty-eight hours after transfection, medium was removed and replaced with fresh CDI maintenance media. AAV transduction at a MOI, multiplicity of infection, often occurred at the time of media change. After overnight incubation with AAV, media was replaced next day.

Evaluation of contractility and electrical signals of iPSC-CMs

Contraction of iPSC-CM was recorded in bright field by SONY S18000 imaging system and acquired videos were analyzed by DANA Solutions Pulse analysis software (now Curi Bio). Contraction was recorded daily from day 3 to day 8 post AAV transduction and day 5 to day 10 post siRNA treatment. Each siRNA treatment included 6 to 9 wells on three independent 96-well plates. Contraction velocity was an average of all wells from the same treatment from the same plate. Averaged numbers of contraction velocity were plotted for each of the three plates from day 3 to day 8 post AAV transduction. Beat period, amplitude, and propagation of electrical signal were detected as extracellular field potential signals from the cardiac monolayers using Axion Biosystems Microelectrode array (MEA) plates (Navarrete et al., 2013). Cell seeding and maintenance on 12, 24, or 96-well plates followed the manufacturer's recommendation. Data were collected at the time points and analyzed the same way as the contraction velocity.

Immunofluorescence imaging of iPSC-CMs

Cells were fixed in 4% paraformaldehyde for 15 min and permeabilized with PBS + 0.1% Triton-X100 (PBST) at room temperature for 15 min. Cells were washed with PBS three times followed by blocking with PBST + 4% bovine serum albumin (BSA) for 1 h. Cells then were incubated with antibodies against anti-PKP2 (Invitrogen, rabbit polyclonal PA5-53144) at 1:200 dilutions or anti-DSP (Invitrogen, rabbit polyclonal 25318-1-AP; Sigma, mouse monoclonal MABT1492) at 1:100 dilutions or anti-JUP (Sigma, mouse monoclonal P8087) at 1:200 dilutions in PBS + 4% BSA for overnight. After washing with PBS three times, cells were then incubated with donkey anti-mouse or anti-rabbit Alexa Fluor 488, 594 or 647 (Invitrogen) at 1:500 dilutions in PBS + 4% BSA for 2 h. Cells were imaged on Molecular Devices ImageXpress Micro

Confocal High-Content Imaging System and quantified using MetaXpress imaging analysis software.

Echocardiography

Transthoracic echocardiography was performed using high resolution micro-imaging systems (Vevo 3100 Systems, Fujifilm VisualSonics) equipped with a 25-55 MHz linear array transducer for mouse heart images acquisition. Briefly, lightly anesthetized spontaneously breathing mice (1-1.5% isoflurane and 98.5-99% O_2) were placed in the supine position on a temperature-controlled heating platform to maintain their body temperature at ~37°C. Parasternal long-axis B-mode tracings of right ventricular outflow track (RVOT) were recorded for RV area measurement, parasternal short-axis M-mode tracings of left ventricle (LV) were recorded for left ventricle internal diameter in end diastole (LVIDd) and LV ejection fraction (EF) calculation.

Electrocardiogram recordings

Mice were anesthetized with 1-1.5% isoflurane and 98.5-99% O_2 via a nose cone (following induction in a chamber containing isoflurane 4–5% in oxygen). Rectal temperature was monitored continuously and maintained at 37–38 °C using a heat pad. Two lead ECG (leads II) were recorded from sterile electrode needles (29-gauge) inserted subcutaneously into the right upper chest with the negative electrode needle and into the left bottom chest with the positive electrode needle. The signal was then acquired and analyzed using a digital acquisition and analysis system (Power Lab; AD Instruments; LabChart 7 Pro software version). ECG parameters (QT interval) were quantified after 1–2 min from the stabilized trace. For spontaneous arrhythmias monitoring, mice were monitored for 30 min after anesthesia induction.

Mouse Histology

Mice were anesthetized with ketamine xylazine cocktail. First, mice were perfused transcardially with PBS. A scalpel was used to cut hearts into two along the coronal plane and drop-fixed overnight in 10% formalin. Fixed heart tissues were sent to Histowiz for trichrome staining and quantification of fibrosis and immunohistochemical staining of PKP2 and Cx43 using rabbit anit-PKP2 and rabbit anti-Cx43 (PA5-53144 and 71-0700).

Cardiac transduction, mRNA, protein analysis

For cardiac vector genomes analysis, DNA was extracted using the DNeasy Blood and Tissue Kit (Qiagen Sciences, 69506). Absolute quantification of cardiac viral genomes per microgram of genomic DNA was assessed by qPCR using a WPRE gBlock (IDT) as a DNA standard across six orders of magnitude. WPRE gBlock sequence is CCTGGTTGCTGTCTCTTTATG AGGAGTTGTGGCCCGTTGTCAGGCAACGTGGCGTGGTGTGCACTGTGTTTGCTGACGCAA CCCCCACTGGTTGGGGCATTGCCACCACCTGTCAGCTCCTTTCCGGGACTTTCGCTTTCC CCCTCCCTATTGCCACGGC. Corresponding primers and probes for qPCR are WPREqpcr_ F1: 5' CCG TTG TCA GGC AAC GTG 3'; WPREqpcr_R1: 5' AGC TGA CAG GTG GTG GCA AT 3'; and Probe: FAM/TGC TGA CGC AAC CCC CAC TGG T/TAMSp.

Total RNA was extracted from iPSC-CMs or cardiac RV and LV tissue using the RNeasy Mini or Universal Mini Kit (Qiagen Sciences, 74106 and 73404), cDNA synthesized (Invitrogen SuperScript III First-Strand Synthesis SuperMix for qRT-PCR) and analyzed by qRT-PCR using Taqman probes to human *PKP2* or mouse *Pkp2* gene, heart failure genes (*Nppa, Nppb*), and fibrosis genes (*Col1a1, Col3a1, and Timp1*). Mouse *Gapdh* served as an internal housekeeping gene control. Absolute transgene mRNA copy number was determined by RT-qPCR using a WPRE-specific RNA standard (GenScript) across six orders of magnitude. WPRE RNA standard sequence is mG*UAUAAAUCCUGGUUGCUGUCUCUUUAUGAGGAGUUGUG GCCCGUUGUCAGGCAACGUGGCGUGGUGUGCACUGUGUUUG*mC. Corresponding primers and probe for RT-qPCR are WPREqpcr_F3: 5' GGT TGC TGT CTC TTT ATG AGG AGT T 3'; WPREqpcr_R3: 5' GCA CAC CAC GCC ACG TT 3'; and Probe: FAM/TGG CCC GTT GTC AGG/TAMSp.

Cardiac LV lysates in RIPA lysis buffer were analyzed by immunoblotting with mouse anti-PKP2, rabbit anti-DSP, rabbit anti-JUP, rabbit anti-Cx43, and mouse anti-GAPDH (SC-393711, 25318-1-AP, SAB4501616, 71-0700, and MA5-15738, respectively).

Statistical Guidelines

The number of technical and biological replicates and animals for each experiment are indicated in the figure legends. Statistical analyses were performed using Prism 9. Student's t test was used to analyze two unpaired groups. Significant differences were defined as $P < 0.05$. Error bars in all *in vivo* studies represent SEM (Standard Error of the Mean).

Transcriptional analysis by RNA sequencing

From each replicate, 100 ng total RNA was extracted via the polyA-tail-specific protocol according to Illumina Inc.. RNA quality control was performed before library prep using Agilent TapeStation instrument. The RNA libraries were prepared using a Stranded Total RNA Library Prep with Ribo-Zero Plus kit (Illumina), which also removes ribosomal RNA. The libraries were sequenced as 2x50 base pair paired-end reads using Illumina NovaSeq 6000 using V1.5 reagent kit on S1 flow cell with an average of 25.66 million reads per each read file (51.32M reads per sample). Raw RNA-seq reads from mouse hearts in fastq format were aligned with Salmon (version 1.8.0) to the GENCODE (version M30, July 2022) reference transcript assembly (GRCm39 and Ensembl 107) using best practice parameters to ensure mapping validity and reproducibility (--seqBias --gcBias --posBias --useVBOpt --rangeFactorizationBins 4 --validateMappings --mimicStrictBT2). Next, a script using R package *tximport* was used to generate an expression matrix normalized to transcripts per million (TPM). In this analysis, we only used genes detected in at least 10% of all samples. Protein-coding genes were determined using Ensembl release *mus musculus* annotations (GRCm39, July 2022) and extracted by *biomaRt* (version 2.52.0). Mitochondrial genes were also omitted, followed by renormalization to TPM. These gene expression values were then log2-transformed after addition of 1 as pseudo-count. Expression patterns of key genes associated with functions of interest were visualized across treatment groups with boxplots (Fig. 7f) generated using the *ggplot2* R package. Expression values from both left and right ventricles were included in the boxplots. Relative gene expression levels across groups and two ventricles are also presented in scaled values per gene in the heatmaps (Fig. 7d, 8f). Heatmaps were generated in R using *ComplexHeatmap* package.

For initial assessment and identifying presence of cluster patterns in the transcriptome, Principal Component Analysis (PCA) models were generated in R using the `prcomp` function from the *stats* package. The first two principal components were used to visualize group level differences across samples in a PCA plot (Fig. 8c) generated using *ggplot2* and *ggfortify* packages with the `autoplot` function. Differential gene expression analysis was then performed by comparing each two groups of interest using Welch's *t*-test on pseudo-log normalized TPM values. The obtained *t* statistics values were used to rank-order the genes for the downstream functional analyses. Volcano plots (Fig 7e, 8d) were then generated to visualize the top positive and negative differentially expressed genes (DEGs) using the *ggplot2* R package. The top DEGs are the set of genes with the highest and lowest t-statistics values. To evaluate functional effects, we performed Gene Set Enrichment Analysis (GSEA) (Subramanian et al.,

2005) on the gene list pre-ranked by t-statistics obtained from differential gene expression analysis, using the *clusterProfiler* R package. GSEA assesses whether differences in expression of predefined gene sets between two phenotypes are concordant and statistically significant. Gene sets were obtained from positional, curated canonical pathways, transcription factor targets, Gene Ontology, cell type signatures and Hallmark collections in Human MSigDB (v2023.1.Hs) (Subramanian et al., 2005; Liberzon et al., 2011, Liberzon et al., 2015). Upon performing GSEA, these gene sets were only considered statistically significant if the false discovery rate (Q value) was less than 0.25 as determined with multiple hypothesis testing correction using the BH-correction method (Glickman et al., 2014). The normalized enrichment score, which reflects the degree to which a gene set is overrepresented in the ranked list and normalized for gene set size, was used to select significantly altered gene sets. Trends in normalized enrichment scores for some gene sets of interest were shown in heatmaps (Fig. 8g), which were generated in R using *ComplexHeatmap*.

Reference

Agullo-Pascual E, Cerrone M, and Delmar M. (2014) Arrhythmogenic cardiomyopathy and Brugada Syndrome: diseases of the connexome. FEBS Lett. 588(8): 1322-1330.

Akdis D, Medeiros-Domingo A, Gaertner-Rommel A et al. (2015) Myocardial expression profiles of candidate molecules in patients with arrhythmogenic right ventricular cardiomyopathy/ dysplasia compared to those with dilated cardiomyopathy and healthy controls. Heart Rhythm 13(3):731-741.

Asimaki A, Tandri H, Huang H, *et al.* (2009) A new diagnostic test for arrhythmogenic right ventricular cardiomyopathy. N. Engl. J. Med. 360:1075-1084.

Austin KM, Trembley MA, Chandler SF *et al.* (2019) Molecular mechanism of arrhythmogenic cardiomyopathy. Nat. Rev. Cardiol. 16(9):519-537.

Awad M, Calkins H, and Judge, DP. (2008) Mechanisms of disease: molecular genetics of arrhythmogenic right ventricular dysplasia/cardiomyopathy. Nat. Clin. Pract. Cardiovasc. Med. 5(5): 258-267.

Basso C, Bauce B, Corrado D, Thiene G. (2011) Pathophysiology of arrhythmogenic cardiomyopathy. Nat. Rev. Cardiol. 9:223–33.

Benjamini Y and Hochberg Y. (1995) Controlling the false discovery rate: a practical and powerful approach to multiple testing. J. R. Stat. Soc. Series B Stat. Methodol. 57(1):289-300.

Cerrone M, Noorman M, Lin X *et al.* (2012) Sodium current deficit and arrhythmogenesis in a murine model of plakophilin-2 haploinsufficiency. Cardiovasc Res. 95(4):460-468.

Cerrone M, Montnach J, Lin X *et al.* (2017) Plakophilin-2 is required for transcription of genes that control calcium cycling and cardiac rhythm. Nat. Commun. 8, 106.

Chen SN, Gurha P, Lombardi R, Ruggiero A, Willerson JT, and Marian AJ. (2014) The Hippo pathway is activated and is a causal mechanism for adipogenesis in arrhythmogenic cardiomyopathy. Circ. Res. 114(3): 454-468.

Choudhary N, Tompkins C, Polonsky B, Mcnitt S, Calkins H, Estes, III, NAM, Krahn AD, Link MS, Marcus FI, Towbin JA, and Zareba W, M.D., *et al*. (2016) Clinical presentation and outcomes by sex in arrhythmogenic right ventricular cardiomyopathy: findings from the north American ARVC Registry. J. Cardiovasc. Electrophysiol. 27(5): 555–562.

Delmar M and McKenna WJ. (2010) The cardiac desmosome and arrhythmogenic cardiomyopathies: from gene to disease. Cir. Res. 107(6):700-714.

Dries AM, Kirillova A, Reuter CM, Garcia J, Zouk H, Hawley M, Murray B, Tichnell C, *et al.*. (2021) The genetic architecture of Plakophilin 2 cardiomyopathy. Genet. Med. 23(10): 1961–1968.

Dubash AD, Kam CY, Aguado BA, Patel DM, Delmar M, Shea LD, and Green KJ. (2016) Plakophilin-2 loss promotes TGF-β1/p38 MAPK-dependent fibrotic gene expression in cardiomyocytes. J. Cell Biol. 212(4): 425-438.

Edelberg, J.M., Sehnert, A.J., Mealiffe, M.E. *et al.* (2022) The Impact of Mavacamten on the Pathophysiology of Hypertrophic Cardiomyopathy: A Narrative Review. Am. J. Cardiovasc Drugs 22, 497–510.

Finocchiaro G, Papadakis M, Robertus JL, Dhutia H, Steriotis AK, Tome M, Mellor G, Merghani A, Malhotra A, Behr E, *et al*. (2016) Etiology of sudden death in sports: insights from a United Kingdom Regional Registry. J. Am. Coll. Cardiol. 67:2108–2115.

Gerull B, Heuser A, Wichter T, *et al*. (2004) Mutations in the desmosomal protein plakophilin-2 are common in arrhythmogenic right ventricular cardiomyopathy. Nat. Genet. 36(11):1162-1164.

Hayes, H.B., Nicolini, A.M., Arrowood, C.A. *et al.* (2019) Novel method for action potential measurements from intact cardiac monolayers with multiwell microelectrode array technology. Sci. Rep. 9, 11893.

Hug N, Longman D, and Cáceres JF. (2016) Mechanism and regulation of the nonsense-mediated decay pathway. Nucleic Acids Res. 44(4):1483-1495.

Jacob KA, Noorman M, Cox MG, Groeneweg JA, Hauer RN, van der Heyden MA. (2012) Geographical distribution of plakophilin-2 mutation prevalence in patients with arrhythmogenic cardiomyopathy. Neth. Heart J. 20(5):234-9.

Jolliffe Ian T. and Cadima Jorge. (2016) Principal component analysis: a review and recent developments. Phil. Trans. R. Soc. A.374 20150202.

Kohela A, Van Kampen SJ, Moens T, *et al.* (2021) Epicardial differentiation drives fibro-fatty remodeling in arrhythmogenic cardiomyopathy. Sci. Transl. Med. 13(612): eabf2750.

Kowalczyk AP and Green KJ. (2013) Structure, function and regulation of desmosomes. Prog. Mol. Biol. Transl. Sci. 2013; 116: 95–118.

Larosche I, Lettéron P, Fromenty B, Vadrot N, Abbey-Toby A, Feldmann G, Pessayre D, Mansouri A. (2007) Tamoxifen inhibits topoisomerases, depletes mitochondrial DNA, and triggers steatosis in mouse liver. J. Pharmacol. Exp. Ther. 321(2):526-35.

Liberzon, A. et al., Stecyna, J. *et al.* (2011) Molecular signatures database (MSigDB) 3.0. Bioinformatics, 27(12), 1739-1740.

Liberzon, A. *et al.* (2015) The molecular signatures database hallmark gene set collection. Cell systems, 1(6), 417-425.

Maddah M., Heidmann J. D., Mandegar M. A., Walker C. D., Bolouki S., Conklin B. R., *et al.* (2015) A non-invasive platform for functional characterization of stem-cell-derived cardiomyocytes with applications in cardiotoxicity testing. Stem. Cell. Rep. 4 621–631.

Mura IEAL, Bauce B, Nava A *et al.* (2013) Identification of a PKP2 gene deletion in a family with arrhythmogenic right ventricular cardiomyopathy. Eur. J. Hum. Genet. 11 :1226-1231.

Nava A, Bauce B, Basso C, Muriago M, Rampazzo A, Villanova C, Daliento L, Buja G, Corrado D, Danieli GA, Thiene G. (2000) Clinical profile and long-term follow-up of 37 families with arrhythmogenic right ventricular cardiomyopathy. J. Am. Coll. Cardiol. 36:2226–33.

Navarrete EG, Liang P, Lan F, Sanchez-Freire V, Simmons C, Gong T, Sharma A, Burridge PW, Patlolla B, Lee AS, Wu H, Beygui RE, Wu SM, Robbins RC, Bers DM and Wu JC. (2013) Screening drug-induced arrhythmia [corrected] using human induced pluripotent stem cell-derived cardiomyocytes and low-impedance microelectrode arrays. Cir. 128:S3–13.

Navarro KL, Huss M, Smith JC, Sharp, Marx JO, Pacharinsak C. (2021) Mouse Anesthesia: The Art and Science. ILAR Journal 62(1-2): 238-273.

Oxford EM, Musa H, Maass K *et al.* (2007) Connexin43 remodeling caused by inhibition of Plakophilin-2 expression in cardiac cells. Cir. Res. 101:703-711.

Rasmussen TB, Nissen PH, Palmfeldt J *et al*. (2014) Truncating Plakophilin-2 mutations in arrhythmogenic cardiomyopathy are associated with protein haploinsufficiency in both myocardium and epidermis. Circ: Cardiovascular Genetics 7:230-240.

Reichart D, Lindberg EL, Maatz H, *et al*. (2022) Pathogenic variants damage cell composition and single-cell transcription in cardiomyopathies. Science 377:619.

Reid CA, Boye SL, Hauswirth WW, Lipinski DM. (2017) miRNA-mediated post-transcriptional silencing of transgene leads to increased adeno-associated viral vector yield and targeting specificity. Gene Ther. 24:462-469

Ribeiro MPC, Santos, AE, Custódio, JBA. (2014) Mitochondria: the gateway for tamoxifen-induced liver injury. Toxicology 323:10-8.

Rodríguez-Sinovas A; Sánchez, JA, Valls-Lacalle L, Consegal M and Ferreira-González I. (2021) Connexins in the heart: regulation, function and involvement in cardiac disease. Int. J. Mol. Sci. 22: 4413.

Sheikh F, Ross RS, and Chen J. (2009) Cell-cell connection to cardiac disease. Trends Cardiovasc. Med. 19(6):182-190.

Song J-P, Chen L, Chen X *et al.* (2020) Elevated plasma β-hydroxybutyrate predicts adverse outcomes and disease progression in patients with arrhythmogenic cardiomyopathy. Sci. Transl. Med. 12(530): eaay8329.

Subramanian, A. *et al.* (2005) Gene set enrichment analysis: a knowledge-based approach for interpreting genome-wide expression profiles. Proc. Natl. Acad. Sci. USA 102(43), 15545-15550.

Towbin JA, McKenna WJ, Abrams DJ, *et al*. (2019) HRS expert consensus statement on evaluation, risk stratification, and management of arrhythmogenic cardiomyopathy. Heart Rhythm 2019; 16:e301.

van Opbergen CJ, Noorman M, Pfenniger A *et al.* (2019) Plakophilin-2 haploinsufficiency causes calcium handling deficits and modulates the cardiac response towards stress. Int. J. Mol. Sci. 20: 4076.

Vermij SH, Abriel H, van Veen TA. (2017) Refining the molecular organization of the cardiac intercalated disc. Cardiovasc Res. 113(3):259-275.

Walsh R, Thomson KL, Ware JS, *et al.* (2017) Reassessment of mendelian gene pathogenicity using 7,855 cardiomyopathy cases and 60,706 reference samples. Genetics in Med. 19 (2):192-203.

Zhang J., Liang Y, Bradford WH, and Sheikh F. (2021) Desmosomes: emerging pathways and non-canonical functions in cardiac arrhythmias and disease. Biophys. Rev. 13:697-706.

Acknowledgement

We thank Dr. Mario Delmar and NYU for licensing *Pkp2-cKO* mouse.

We thank our vivarium team for taking care of animals, Xiaomei Song, Cristina Dee-Hoskins, Carolina Gomez Gutierrez, Jessie Madariaga, Kevin Robinson, Yolanda Hatter.

Main Figures-Legends

Figure 1. siRNA-mediated PKP2 acute silencing impacted both cellular structure and functions of human iPSC-CMs.

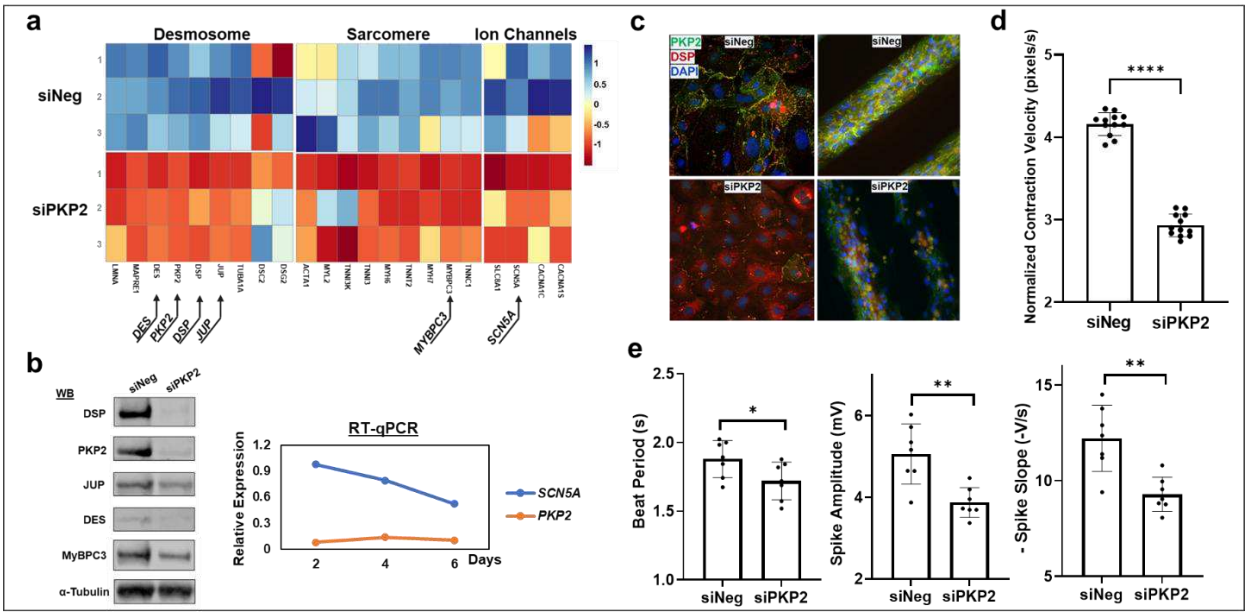

a, Heatmap of RNA sequencing analyses (n = 3) from iPSC-CMs (n=3) harvested 6 days after treatment with siRNAs against PKP2 (siPKP2) or negative control siRNAs (siNeg) highlighting effects on genes encoding components of the desmosome, sarcomere, and ion channels. **b,** PKP2 silencing led to reduction in protein expression of DSP, JUP, DES, and MyBPC3 in response to reduced PKP2 protein (Western blot on the left panel) and reduction in *SCN5A* mRNA in response to reduced *PKP2* mRNA (RT-qPCR on the right panel). **c,** PKP2 silencing resulted in disappearance of PKP2 and DSP protein from the cellular membrane (left two panels) and cell-to-cell disarray in patterned iPSC-CMs (right two panels). Immunofluorescent staining: PKP2 in green, DSP in red, and nuclei in blue. **d,** PKP2 silencing led to defective contraction as quantified by contraction velocity using Pulse video analysis (Maddah et al., 2015) (Curi Bio). Average nuclear counts from live cells were used to normalize contraction velocity. **e**, PKP2 silencing led to depressed beat period, amplitude, and rate of propagation of electrical signal detected as extracellular field potential signals from the cardiac monolayers using Microelectrode array (MEA) plates (Hayes, et al., 2019) (Axion Biosystems).

Figure 2. AAV:hPKP2 transgene restored the expression level of DSP protein and rescued contraction velocity post PKP2 silencing in human iPSC-CMs.

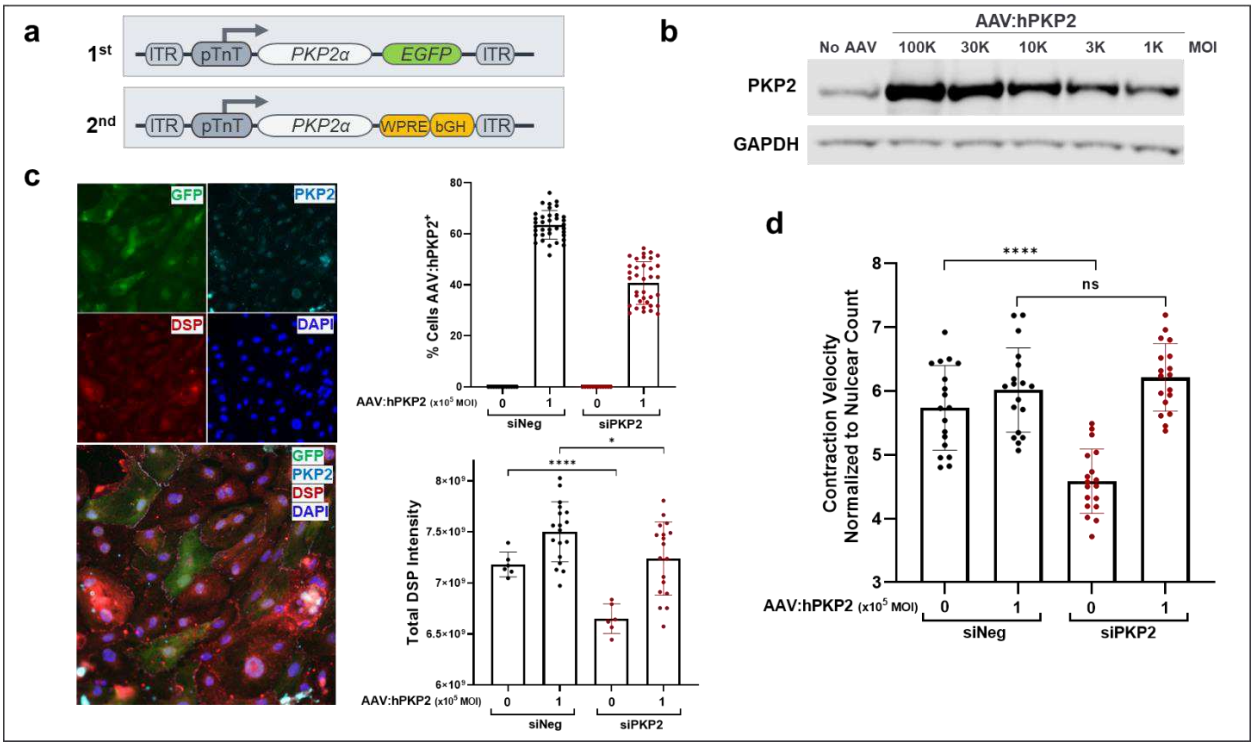

a, Schematic representation of the 1st generation and the 2nd generation AAV expression cassette of PKP2α. Key 3' elements in AAV expression cassette include Woodchuck hepatitis virus post-transcriptional regulatory element (WPRE), and bovine growth hormone polyadenylation signal (bGH). **b,** Western blot analysis showed that the second generation of AAV:hPKP2 is expressed in iPSC-CMs in a dose-dependent fashion by applying viruses at different multiplicity of infection (MOI). **c,** GFP expression in the first generation of PKP2 expression cassette was used to label AAV transduced iPSC-CMs. The immunofluorescent mini panels show cells were stained for GFP, PKP2, DSP and nuclei, respectively, with the bottom large panel showing merged channels. The top bar graph summarized the percentage of cells expressing GFP. The bottom graph showed restored DSP protein expression quantified by DSP immunofluorescent signal post PKP2 silencing in the absence or the presence of AAV:hPKP2 transgene, which was not silenced by siRNAs. Intensity of DSP immune-fluorescent signal was quantified at day 10 of PKP2 silencing and day 8 of AAV transduction. **d,** AAV:hPKP2 showed a rescue of contraction velocity post PKP2 silencing in iPSC-CMs. Cell contractility was recorded from day 3 to 8 post AAV transduction and analyzed by Pulse video analysis. Average nuclear counts from live cells were used to normalize contraction velocity. For each treatment, contraction velocity was an average of 6 to 9 wells on three independent 96-well plates from day 3 to day 8 post AAV transduction. Statistical significance is estimated by Student t-test with p-value at ****p<0.001, ***p<0.01, *p<0.05, and not significant (ns).

Figure 3. *Pkp2-cKO* ARVC mouse model recapitulated the majority of human ARVC clinical manifestations.

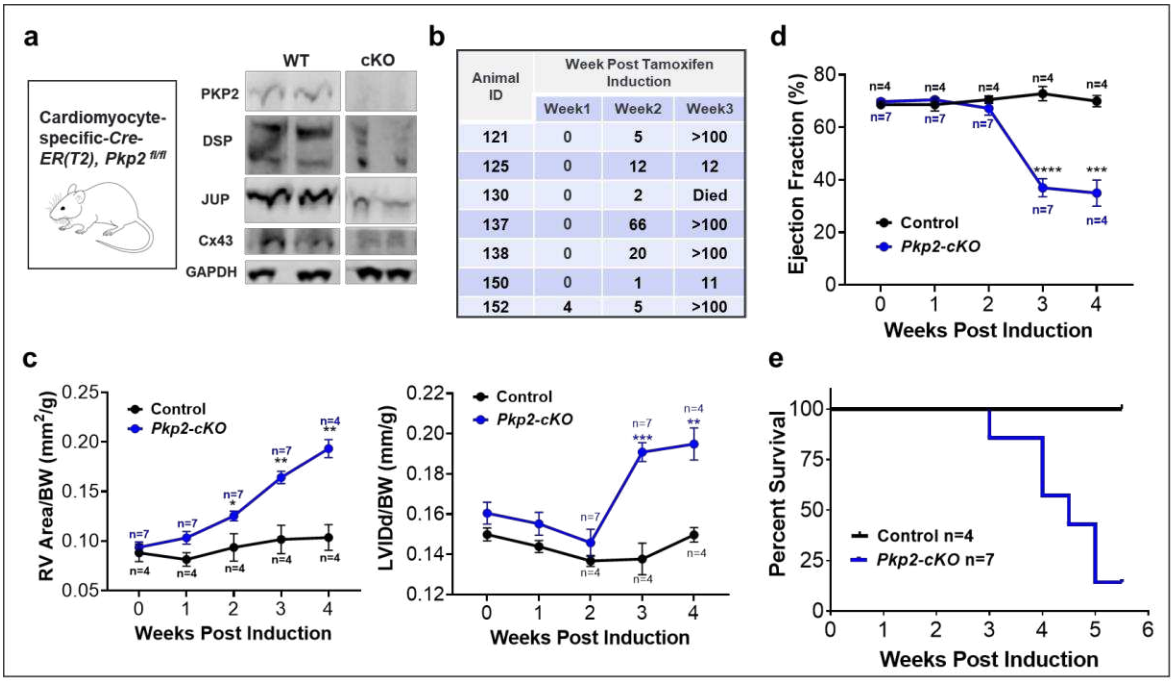

a, *Pkp2-cKO* ARVC mice (*αMyHC-Cre-ER(T2), Pkp2* $^{fl/fl}$) at ~3 months of age were injected with tamoxifen to induce cardiac knock-out of the *Pkp2* gene. Representative immunoblots showed reduction of desmosome proteins PKP2, DSP, PKG, and GJ protein Cx43. **b,** *Pkp2-cKO* mice developed spontaneous PVCs as observed during 30 minutes of continuous recording of EKG. **c,** *Pkp2-cKO* mice started to develop biventricular dilatation at 2 weeks post tamoxifen induction. RV area (left panel) and LV internal diameter end diastole (LVIDd, right panel) were normalized to body weight. **d,** LV performance measured by % ejection fraction sharply declined at 2 weeks post tamoxifen induction. **e,** Kaplan-Meier survival curve showed a sharp decline of survival of *Pkp2-cKO* mice beginning 3 weeks post tamoxifen induction. Animals showed severe symptoms including sudden death, edema, reduced activity, and reduced tolerance to isoflurane beginning 3 weeks post induction. P value: Student's t-test. Error bar: s.e.m.; *p<0.05, **p<0.01, ***p<0.001, ****p<0.0001 vs. WT.

Figure 4. An early and single dose of AAV9:PKP2 significantly reduced arrhythmias, improved cardiac function, and prolonged median lifespan to ≥ 58 weeks post AAV administration.

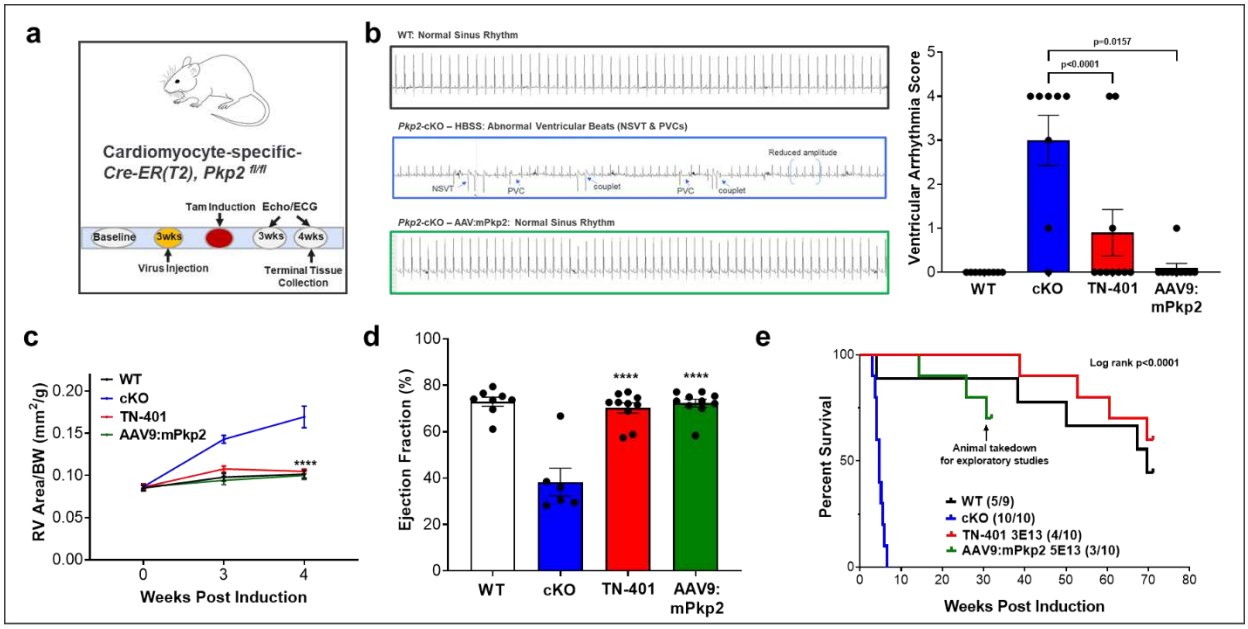

a, Study design to evaluate TN-401 or AAV9:mPkp2 efficacy using *Pkp2-cKO* ARVC mouse model. AAV9 was injected three weeks before gene deletion, TN-401 at 3E13 vector genomes per kilogram bodyweight (vg/kg) and AAV9:mPkp2 at 5E13 vg/kg. Echocardiograph (Echo) and electrocardiogram (EKG) data were collected at week 3 and week 4 post gene deletion. **b,** Raw EKG traces showed a significant contrast in spontaneous arrhythmias in *Pkp2-cKO* mice in the absence and the presence of AAV9:mPKP2 treatment. PVCs, premature ventricular contractions; NSVT, non-sustained ventricular tachycardia. The right graph summarized averaged arrhythmia scores representing frequency, duration, and severity of ventricular arrhythmias. AAV9:PKP2 treatment resulted in significantly improved arrhythmia scores. **c,** AAV9:PKP2 treatment of *Pkp2-cKO* mice showed efficacy in reducing RV dilation as estimated by RV area normalized to body weight (mm^2/g) and **d,** maintaining left ventricular ejection fraction at 4 weeks post gene deletion. **e,** Kaplan-Meier survival curve showed that TN-401 extended median lifespan of *Pkp2-cKO* mice by ≥ 58 weeks post gene deletion. Numbers in paratheses showed dead vs live animals by the time of takedown. Animals treated by AAV9:mPkp2 (in green line) were taken down early for exploratory studies. P value: Student's t-test. Error bar: s.e.m.; ****, p<0.0001.

Figure 5. TN-401 dose-dependently reduced arrhythmias, improved heart structure and cardiac function, restored expression of desmosome proteins and Cx43 and prevented development of fibrosis in *Pkp2-cKO* mouse.

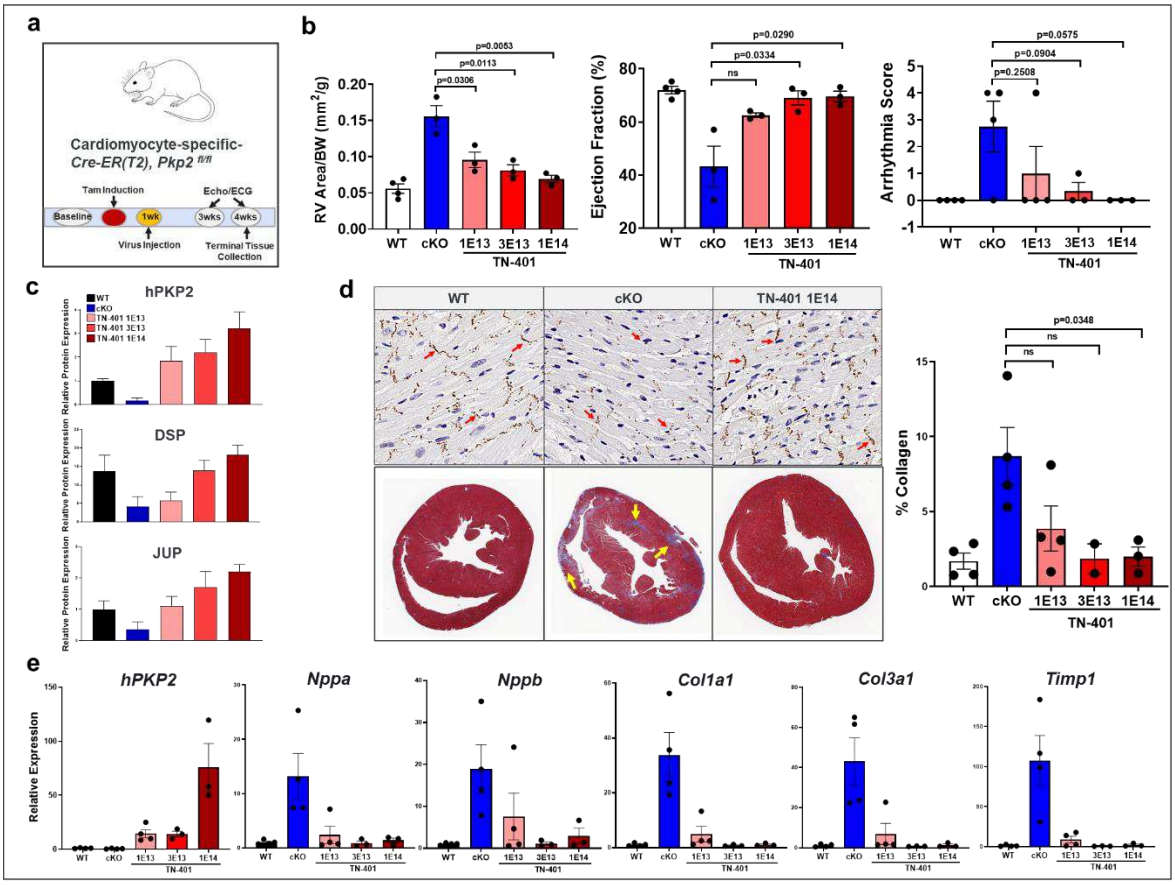

a, Study design to evaluate dose-dependent efficacy of TN-401 using *Pkp2-cKO* ARVC mouse model. Mice were injected with TN-401 at 1E13, 3E13, or 1E14 vg/kg at one week after tamoxifen induction of cardiac *Pkp2* gene deletion. At 4 weeks post tamoxifen induction (3 weeks post AAV9 injection), animals were sacrificed for expression and histological evaluation. **b,** TN-401 showed dose-dependent efficacy at 3 weeks in preventing RV dilation (mm^2/g), preventing decline of % LV ejection fraction, and trending improvement in arrhythmia scores. **c,** Semi-quantitative Western blot analyses showed restoration of PKP2, JUP, and DSP protein at 3 weeks post AAV treatment. **d,** Immunohistochemistry for the gap junction protein, connexin 43 (Cx43), in heart tissue sections showed restoration of Cx43 expression at intercalated discs (ID) at 3 weeks post AAV treatment (top panels). Red arrows indicate ID. Trichrome staining showed a significant reduction of fibrosis, muscle (red) and fibrosis (blue), in heart sections at 3 weeks post AAV treatment (bottom panel). Yellow arrows highlight areas with fibrosis in *Pkp2-cKO* mouse heart. The percentage of collagen-positive tissue was quantified and shown in the right graph. **e,** RT-qPCR analyses of RV tissue at 3 weeks post AAV treatment showed a dose-dependent expression of *hPKP2* transgene and a dose-dependent suppression of heart failure markers (*Nppa, Nppb*) and fibrosis genes (*Col1a1, Col3a1, Timp1*). *Gapdh* was used as internal control. P value: Student's t-test. Error bar: s.e.m..

Figure 6. A single dose of AAV9:PKP2 after overt cardiomyopathy halted disease progression via reversed adverse right ventricular remodeling, improved LV function, prevented arrhythmia worthening, and reduced mortality.

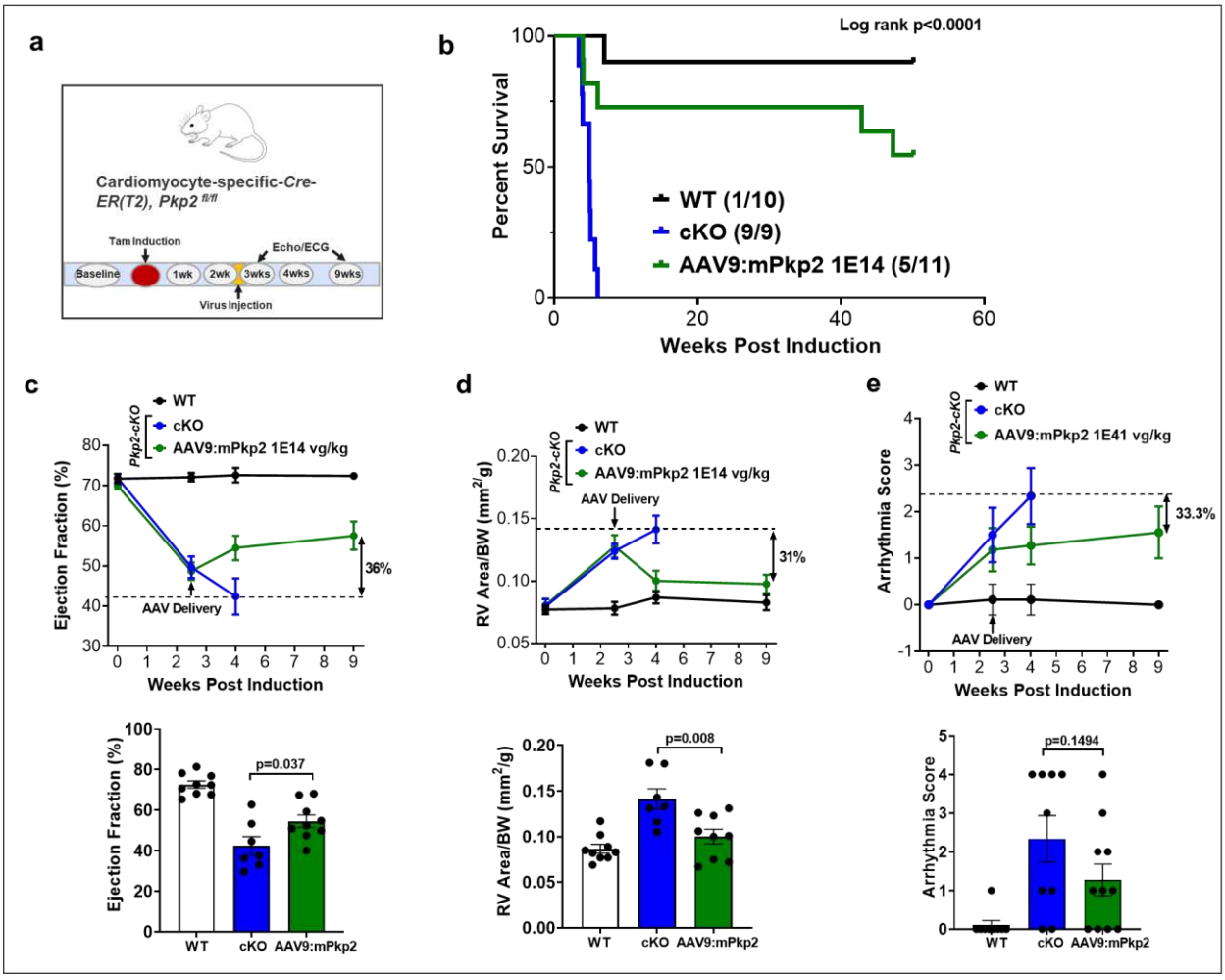

a, Study design to evaluate AAV9:mPkp2 efficacy using *Pkp2-cKO* ARVC mouse model with delivery at 2.5 weeks after *Pkp2* cardiac gene deletion by tamoxifen induction. **b,** HBSS-treated *Pkp2-cKO* ARVC mice died within 6 weeks of cardiac *Pkp2* gene deletion, in contrast, AAV9:mPkp2 treatment significantly reduced mortality and extended median lifespan of *Pkp2-cKO* mice by ≥ 50 weeks. Numbers in paratheses show dead vs live animals by the time of takedown. AAV9:mPkp2 at 9 weeks post gene deletion and 6.5 weeks post treatment **c,** improved left ventricle ejection fraction by 36%; **d,** reversed right ventricle enlargement by 31% and restored RV size similar to that of WT animals (mm^2/g); **e,** prevented further worsening of arrhythmias by 33.3%, all three readouts relative to HBSS treated *Pkp2-cKO* ARVC mice. The bottom bar graphs show EF%, RV size, and arrhythmia score at 4 weeks post gene deletion and 1.5 weeks post treatment. P value: Student's t-test. Error bar: s.e.m..

Figure 7. TN-401 restored expression of genes encoding desmosome, sarcomere, and Ca^{2+} handling system and attenuated expression of genes encoding adverse remodeling factors in a highly coordinated and quantitative fashion.

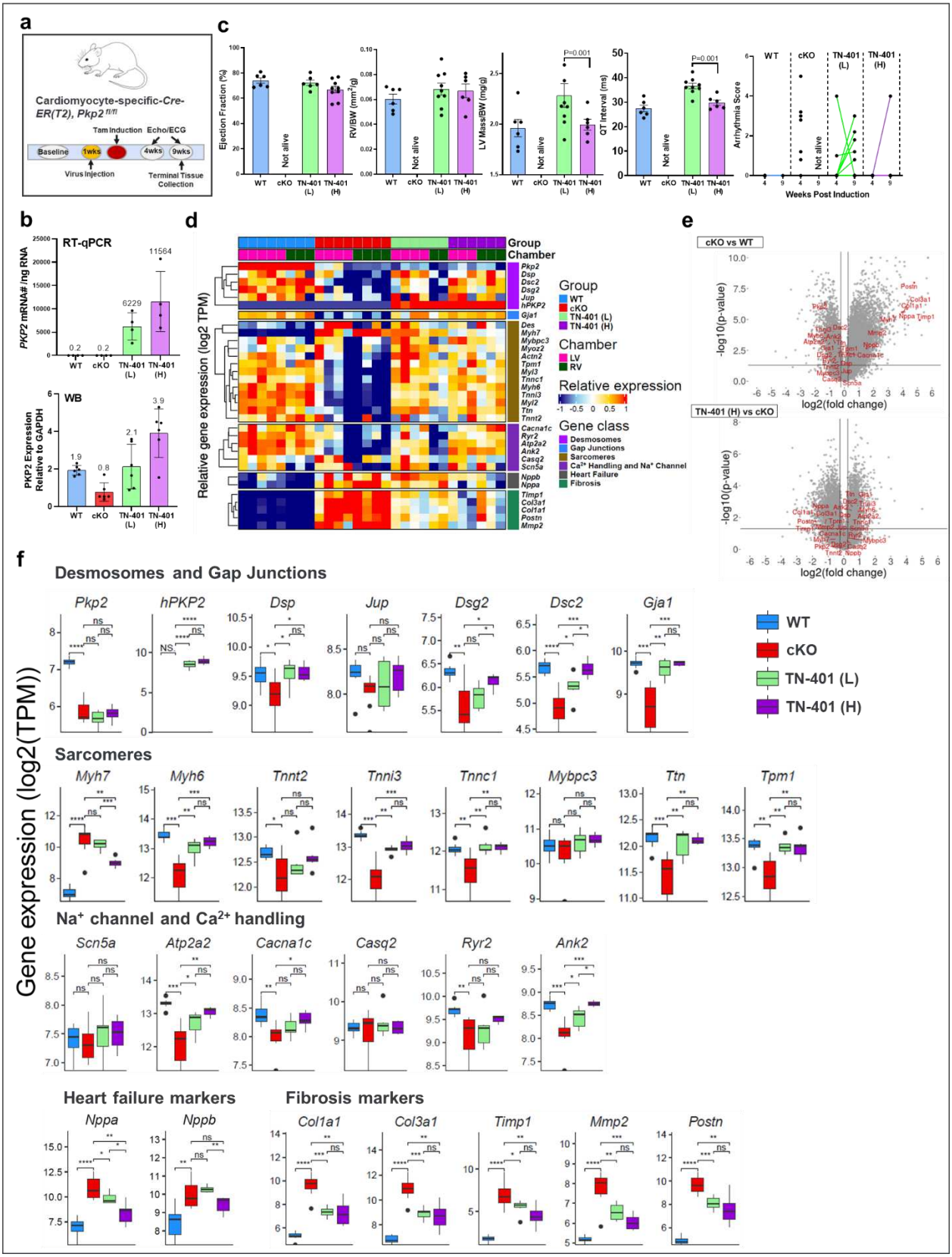
a
Cardiomyocyte-specific-Cre-ER(T2), Pkp2 fl/fl
Tam Induction
Echo/ECG
Baseline
1wks
4wks
9wks
Virus Injection
Terminal Tissue Collection
b
RT-qPCR
PKP2 mRNA# /ng RNA
11564
6229
0.2
0.2
WT
cKO
TN-401 (L)
TN-401 (H)
WB
PKP2 Expression Relative to GAPDH
1.9
0.8
2.1
3.9
c
Ejection Fraction (%)
RV/BW (mm²/g)
LV Mass/BW (mg/g)
QT Interval (ms)
Arrhythmia Score
Not alive
P=0.001
Weeks Post Induction
d
Relative gene expression (log2 TPM)
Group
Chamber
Pkp2
Dsp
Dsc2
Dsg2
Jup
hPKP2
Gja1
Des
Myh7
Mybpc3
Myoz2
Actn2
Tpm1
Myl3
Tnnc1
Myh6
Tnni3
Myl2
Ttn
Tnnt2
Cacna1c
Ryr2
Atp2a2
Ank2
Casq2
Scn5a
Nppb
Nppa
Timp1
Col3a1
Col1a1
Postn
Mmp2
Group
WT
cKO
TN-401 (L)
TN-401 (H)
Chamber
LV
RV
Relative expression
Gene class
Desmosomes
Gap Junctions
Sarcomeres
Ca²⁺ Handling and Na⁺ Channel
Heart Failure
Fibrosis
e
cKO vs WT
TN-401 (H) vs cKO
-log10(p-value)
log2(fold change)
f
Desmosomes and Gap Junctions
Sarcomeres
Na⁺ channel and Ca²⁺ handling
Heart failure markers
Fibrosis markers
Gene expression (log2(TPM))
WT
cKO
TN-401 (L)
TN-401 (H)

a, Study design to evaluate TN-401 dose-dependent efficacy at week 4 and 9 post tamoxifen induction of *Pkp2* gene deletion in *Pkp2-cKO* ARVC mouse model. Animals were dosed by TN-401 at 1 week before induction. **b,** Human *PKP2* transgene mRNA levels at two doses (Low (L), 3E13 vg/kg; High (H), 6E13 vg/kg) were quantified in copy number per ng of total LV RNA (top panel). Human PKP2 transgene protein levels at two doses were compared to the levels of endogenous mouse Pkp2 in WT and in *Pkp2-cKO* mouse post cardiac gene deletion by semi-quantitative Western blot (WB) (bottom panel). **c,** TN-401 treatment at the low (L, 3E13 vg/kg) and high (H, 6E13 vg/kg) dose at week 9 post gene deletion showed comparable efficacy in EF% and RV area (mm^2/g, normalized to body weight) and showed differences in LV mass (mg/g, normalized to body weight), QT intervals, and numbers of animals with arrhythmias. **d,** Heatmap of gene expression was sorted by treatment groups, heart chambers (LV vs RV), and gene classes. Values were presented in scaled log2-transformed. **e,** Volcano plots from differential gene expression (DGE) analysis showed changes between cKO vs WT (WT as reference) (top graph) and TN-401 high dose vs cKO (cKO as reference) (bottom graph). The X-axis represented log2 of fold change in gene expression, and Y-axis showed the negative log10 p-values obtained from DGE analysis for each gene. Genes highlighted in red were selected from each gene class shown in panel d. **f,** Boxplots showed group-wise gene expression for each representative gene of the selected gene classes. Each box showed the distribution of expression values in the following manner: the midline represented the median expression value, the box indicated the interquartile range where the middle 50% of values lie, and the whiskers at the top and bottom of each box represented the range of values outside the interquartile range. Values were in log2 transformed TPM and were aggregated from LV and RV. Comparison p values were calculated by Student's t-test, **** 0 - 0.0001; *** 0.0001 - 0.001; ** 0.001 - 0.01; * 0.01 - 0.05; ns 0.05-1.

Figure 8. Long-term durable expression of AAV9:mPkp2 significantly reduced mortality after disease onset and sustained a broad spectrum of pathways that were perturbed in *Pkp2-cKO* ARVC mouse and restored by the gene therapy.

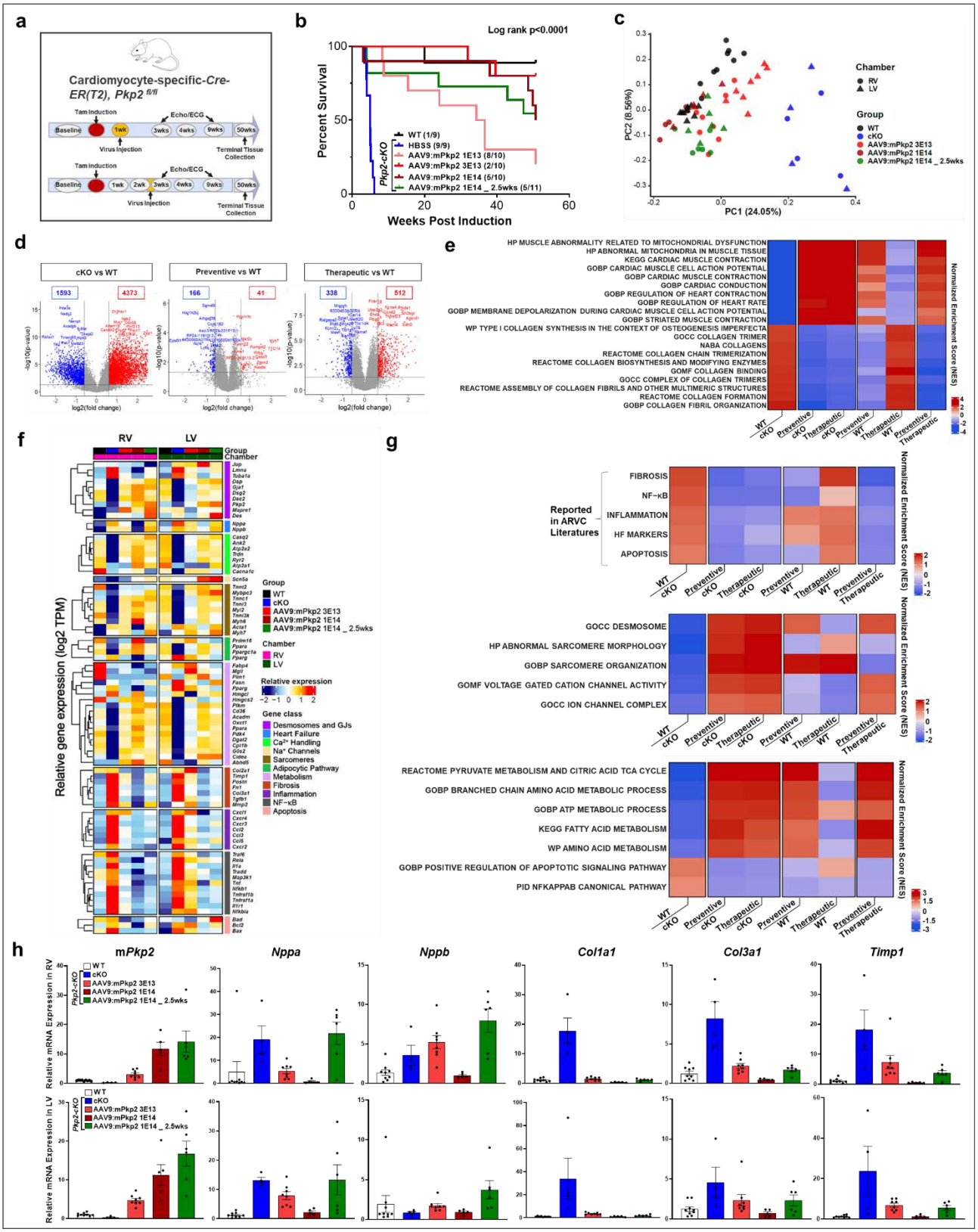
a
Cardiomyocyte-specific-Cre-ER(T2), Pkp2 fl/fl
Tam Induction
Echo/ECG
Baseline
1wk
3wks
4wks
9wks
50wks
Virus Injection
Terminal Tissue Collection
2wk
b
Log rank p<0.0001
Percent Survival
Weeks Post Induction
Pkp2-cKO
WT (1/9)
HBSS (9/9)
AAV9:mPkp2 1E13 (8/10)
AAV9:mPkp2 3E13 (2/10)
AAV9:mPkp2 1E14 (5/10)
AAV9:mPkp2 1E14 _ 2.5wks (5/11)
c
PC1 (24.05%)
PC2 (8.56%)
Chamber
RV
LV
Group
WT
cKO
AAV9:mPkp2 3E13
AAV9:mPkp2 1E14
AAV9:mPkp2 1E14 _ 2.5wks
d
cKO vs WT
Preventive vs WT
Therapeutic vs WT
1593
4373
166
41
338
512
-log10(p-value)
log2(fold change)
e
HP MUSCLE ABNORMALITY RELATED TO MITOCHONDRIAL DYSFUNCTION
HP ABNORMAL MITOCHONDRIA IN MUSCLE TISSUE
KEGG CARDIAC MUSCLE CONTRACTION
GOBP CARDIAC MUSCLE CELL ACTION POTENTIAL
GOBP CARDIAC MUSCLE CONTRACTION
GOBP CARDIAC CONDUCTION
GOBP REGULATION OF HEART CONTRACTION
GOBP REGULATION OF HEART RATE
GOBP MEMBRANE DEPOLARIZATION DURING CARDIAC MUSCLE CELL ACTION POTENTIAL
GOBP STRIATED MUSCLE CONTRACTION
WP TYPE I COLLAGEN SYNTHESIS IN THE CONTEXT OF OSTEOGENESIS IMPERFECTA
GOCC COLLAGEN TRIMER
NABA COLLAGENS
REACTOME COLLAGEN CHAIN TRIMERIZATION
REACTOME COLLAGEN BIOSYNTHESIS AND MODIFYING ENZYMES
GOMF COLLAGEN BINDING
GOCC COMPLEX OF COLLAGEN TRIMERS
REACTOME ASSEMBLY OF COLLAGEN FIBRILS AND OTHER MULTIMERIC STRUCTURES
REACTOME COLLAGEN FORMATION
GOBP COLLAGEN FIBRIL ORGANIZATION
Normalized Enrichment Score (NES)
WT
cKO
Preventive
Therapeutic
f
RV
LV
Relative gene expression (log2 TPM)
Group
Chamber
Relative expression
Gene class
Desmosomes and GJs
Heart Failure
Ca2+ Handling
Na+ Channels
Sarcomeres
Adipocytic Pathway
Metabolism
Fibrosis
Inflammation
NF−κB
Apoptosis
g
Reported in ARVC Literatures
FIBROSIS
NF−κB
INFLAMMATION
HF MARKERS
APOPTOSIS
GOCC DESMOSOME
HP ABNORMAL SARCOMERE MORPHOLOGY
GOBP SARCOMERE ORGANIZATION
GOMF VOLTAGE GATED CATION CHANNEL ACTIVITY
GOCC ION CHANNEL COMPLEX
REACTOME PYRUVATE METABOLISM AND CITRIC ACID TCA CYCLE
GOBP BRANCHED CHAIN AMINO ACID METABOLIC PROCESS
GOBP ATP METABOLIC PROCESS
KEGG FATTY ACID METABOLISM
WP AMINO ACID METABOLISM
GOBP POSITIVE REGULATION OF APOPTOTIC SIGNALING PATHWAY
PID NFKAPPAB CANONICAL PATHWAY
h
mPkp2
Nppa
Nppb
Col1a1
Col3a1
Timp1
Relative mRNA Expression in RV
Relative mRNA Expression in LV
Pkp2-cKO
WT
cKO
AAV9:mPkp2 3E13
AAV9:mPkp2 1E14
AAV9:mPkp2 1E14 _ 2.5wks

a, Study design to evaluate AAV9:mPkp2 efficacy in reducing mortality at 51 weeks post tamoxifen induction of *Pkp2* deletion in *Pkp2-cKO* ARVC mouse model. AAV9:mPkp2 was dosed at 1E13, 3E13, and 1E14 vg/kg either 1 week before the induction (the preventive mode of treatment) or at 1E14 vg/kg at 2.5 weeks after induction (the therapeutic mode of treatment). **b,** Kaplan-Meier curve showed percent survival for each mode of treatment for 51 weeks post *Pkp2* deletion. Numbers in paratheses show dead vs live animals by the time of takedown. **c,** Principal Component Analysis (PCA) showed clusters of gene transcripts from WT (animals taken down at 51 weeks post induction), untreated *Pkp2-cKO* animals (animals taken down at 4 weeks post induction), and AAV9:mPkp2 treated animals (animals taken down at 51 weeks post induction). Principal components 1 and 2 were visualized in X and Y axes. Numbers in brackets represented variation in the data explained by each PC. **d,** Volcano plots from differential gene expression analysis showed changes between cKO vs WT, preventive vs WT, and therapeutic vs WT. Numbers in boxes represented down-regulated and up-regulated genes in blue and red, respectively. **e,** Top 10 positively and top 10 negatively enriched cardiac gene sets were shown with FDR Q value less than 0.25 in Gene Set Enrichment Analysis (GSEA) of *Pkp2-cKO* vs WT (far left column). These enriched gene sets were used to compare preventive vs *Pkp2-cKO*, therapeutic vs *Pkp2-cKO*, preventive vs WT, therapeutic vs WT, and preventive vs therapeutic. **f,** Relative gene expression of selected genes were measured by RNA-seq. Samples were sorted by treatment groups and RV and LV chambers. Genes were categorized by gene classes. Each column depicted a scaled average across samples of each treatment group. Number of animals in each treatment group used for RNA sequencing were 9 WT, 4 cKO, 2 at 1E13 vg/kg (not included on the Heatmap), 8 at 3E13 vg/kg, 5 at 1E14 vg/kg, and 6 at 1E14 vg/kg (the therapeutic mode) with both RV and LV collected. **g,** GSEA heatmap presented positively and negatively enriched cardiac gene sets in *Pkp2-cKO* vs WT. These enriched gene sets were used to compare preventive vs *Pkp2-cKO*, therapeutic vs *Pkp2-cKO*, preventive vs WT, therapeutic vs WT, and preventive vs therapeutic. The top heatmap showed known gene sets reported in ARVC literature (Figure 7d); middle and bottom heatmaps showed annotated gene sets of Canonical Pathways and Gene Ontology groups from Human MSigDB database (v2023.1.Hs) and had *Q* value < 0.25 (See Methods). **h,** RT-qPCR analyses showed expression of a total of mouse *Pkp2* mRNA (including transgene mRNA), heart failure marker genes, *Nppa*, *Nppb*, and fibrosis genes, *Timp1*, *Col1a1*, and *Col3a1*, in RV (top row) and LV (bottom row) at 51 weeks post *Pkp2* deletion.

Figure 9. TN-401 safety study in WT mouse showed no adverse effects at ≤10X of efficacious dose.

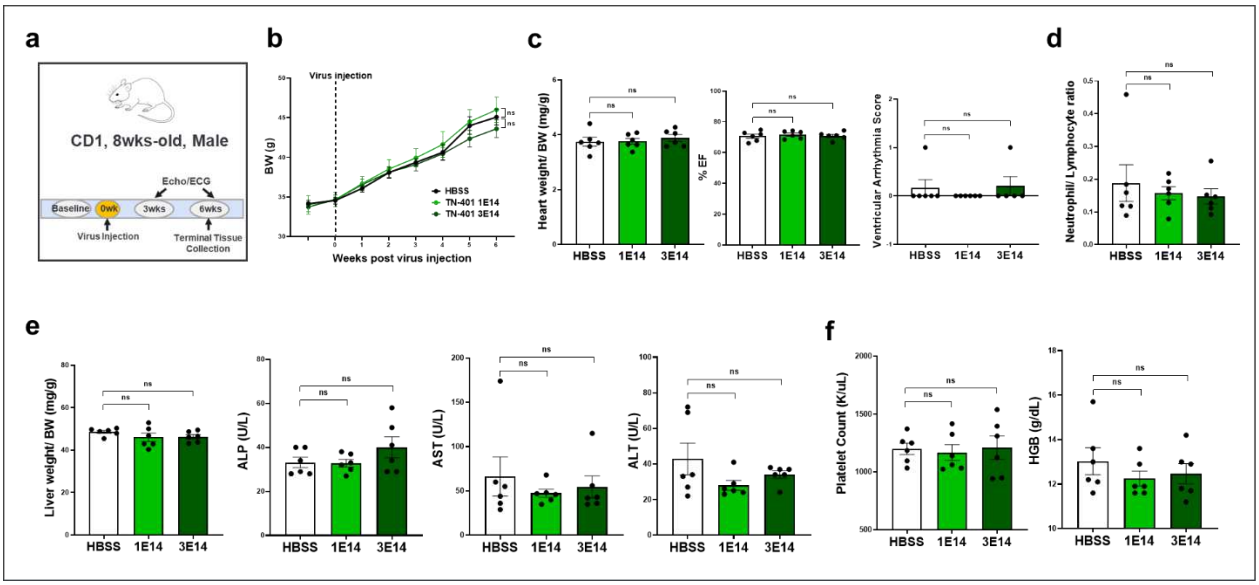

a, Study design to evaluate TN-401 safety in WT CD1 mice. Mice were injected with TN-401 at 1E14 and 3E14 vg/kg, respectively, after baseline readings of body weight, echocardiography, and EKG. Readings post virus injection were recorded at 3 and 6 weeks, respectively, including echocardiography of B-mode, M-Mode (RV, LV), structure (LV internal diameters) and 30-min ECG for quantifying arrythmias and evaluating electrophysiological parameters. Mice were sacrificed in week 6 and tissues and blood samples were collected. **b,** Body weight progression for 6 weeks. **c,** Heart weight normalized to body weight, % ejection fraction (%EF) and ventricular arrhythmia score at 6 wks. **d,** Neutrophil to lymphocyte ratio at 6 wks. **e,** Liver weight normalized to body weight and live function tests, alkaline phosphatase (ALP), aspartate transaminase (AST), alanine transaminase (ALT) at 6 wks. **f,** Platelet counts and hemoglobin (HGB) amount. P value: Student's t-test. Error bar: s.e.m..

Supplementary Files

This is a list of supplementary files associated with this preprint. Click to download.

- SupplementalFigures05192023.pdf